

Rotation and magnetism in intermediate mass stars

Léo G. Quentin,¹[★] Christopher A. Tout²

¹*Département de physique, École normale supérieure, 45 rue d'Ulm, 75005 Paris, France*

²*Institute of Astronomy, University of Cambridge, The Observatories, Madingley Road, Cambridge CB3 0HA*

Accepted XXX. Received YYY; in original form ZZZ

ABSTRACT

Rotation and magnetism are increasingly recognized as important phenomena in stellar evolution. Surface magnetic fields from a few to 20,000 G have been observed and models have suggested that magnetohydrodynamic transport of angular momentum and chemical composition could explain the peculiar composition of some stars. Stellar remnants such as white dwarfs have been observed with fields from a few to more than 10^9 G. We investigate the origin of and the evolution, on thermal and nuclear rather than dynamical time-scales, of an averaged large-scale magnetic field throughout a star's life and its coupling to stellar rotation. Large-scale magnetic fields sustained until late stages of stellar evolution with conservation of magnetic flux could explain the very high fields observed in white dwarfs. We include these effects in the Cambridge stellar evolution code using three time-dependant advection-diffusion equations coupled to the structural and composition equations of stars to model the evolution of angular momentum and the two components of the magnetic field. We present the evolution in various cases for a $3M_{\odot}$ star from the beginning to the late stages of its life. Our particular model assumes that turbulent motions, including convection, favour small-scale field at the expense of large-scale field. As a result the large-scale field concentrates in radiative zones of the star and so is exchanged between the core and the envelope of the star as it evolves. The field is sustained until the end of the asymptotic giant branch, when it concentrates in the degenerate core.

Key words: stars: evolution, stars: general, stars: magnetic fields, stars: rotation, (stars:) white dwarfs

1 INTRODUCTION

While rotation and magnetism have often been considered as minor effects in stellar evolution, observations have shown that these phenomena must be taken into account when describing a star's life. Let us first briefly present the main characteristics of these effects in stars and how magnetic fields in white dwarfs could be linked to the evolution of magnetic fields through stellar evolution processes.

Rotation arises from conservation of angular momentum. Stars form when giant clouds of gas undergo gravitational collapse. Because such clouds have large-scale turbulence, different fluid particles have different velocities, resulting in a non-zero total angular momentum. Therefore, as a cloud collapses and contracts, its material sees its rotation rate increase greatly. When stars eventually form, it is highly likely that they spin around a particular axis. Because of the random nature of turbulence, stars can be found with various angular velocities. So, owing to the centrifugal

force, rotating stars see their hydrostatic balance modified and their structure changed. This is very similar to what can be observed on Earth, where the equatorial radius is approximately 21 km larger than the polar radius. Alongside these structural changes, other effects such as rotationally-driven turbulent mixing or meridional circulation, that is to say from one pole to the other, can also deeply affect the star's chemical evolution. Rotation in stars is very different from Earth's rotation because stars do not necessarily rotate as solid bodies such that material in a star can have different rotation rates at different latitudes and depths, leading to shears. These shears are of particular importance in the development of the instabilities that drive additional mixing.

Stellar magnetism is also a phenomenon that can be observed within our close neighbourhood. The Sun's surface field has a strength of, on average, 1 G. Observations of other stars have shown that the intensity of stellar magnetic fields covers many decades. Some, of type Ap and Bp, have surface fields ranging from 100 to 20,000 G and show chemically peculiar surface compositions compared to normal A type stars. It has therefore been suggested that the

[★] E-mail: leo.quentin@ens.fr

action of magnetic fields has an influence on the composition of these stars. Some elements that are usually present only in the inner parts of stars are radiatively levitated. In short, the strong surface magnetic field stabilizes against turbulence, so that levitation concentrates the heavy elements at the photosphere. Very high magnetic fields are also common features in compact objects. White dwarfs are found with fields ranging between zero to 10^9 G and some magnetic neutron stars can have field strengths of order 10^{15} G. So magnetic effects are present and can be important throughout the life of most stars.

Magnetic fields in stars show very complex behaviour, with structure on small and large scales. The origin of the large-scale fields is still debated. For stars on their main sequence, the phase of their evolution where hydrogen is fused in the core, two possibilities are often considered. They could either be fossil fields, that can be dated back to the star's formation, or fields generated by a dynamo effect, as is thought to be the case in the Sun. In the first case, weak fields within a protostellar gas cloud can become enhanced through flux conservation as the material collapses, giving birth to more intense fields. In the second case, energy is transferred between the kinetic motion of the material in the star to the magnetic field. Large-scale magnetic fields in stars can be unstable, so dynamo effects are highly interesting because they can regenerate these fields.

Hypotheses for the origin of magnetic fields in white dwarfs are the same as those for main-sequence stars. Therefore we wish to know if large-scale fields can be sustained throughout the life of a star, whether they are fossil fields or dynamo generated. White dwarfs are stellar remnants of intermediate- and low-mass stars. At the end of their lives, these stars have completely exhausted the fuel they can burn in their core, which collapses until an equilibrium between gravity and electron degeneracy pressure is reached. White dwarfs emerge as the outer layers of stars are shed by various processes, leaving only the degenerate core. Very high magnetic fields, more than 10^7 G, have been observed in white dwarfs, so one of our motivations is to see if we can obtain such high fields through the evolution of intermediate-mass stars.

We begin by presenting main features of the Cambridge stellar evolution code (STARS) that we use for numerical simulation of stellar evolution, including the model used to describe how both rotation and magnetism have been incorporated in the code in its new version Rotating Stellar Evolution (RoSE) and how exactly we have modified it. We then use the code to derive some results concerning the evolution of the magnetic field in a $3 M_{\odot}$ star for our particular magnetohydrodynamic model. Finally, we briefly present how the evolution of such fields can hint at the origin of the very high magnetic field observed in some white dwarfs.

Most of the theoretical framework in the next sections is based on the dissertation of Potter (2012) and follows the work of Potter, Tout & Eldridge (2012a), Potter, Tout & Brott (2012b), Potter, Chitre & Tout (2012c) and the book *physics, formation and evolution of rotating stars*, by Maeder (2009). The first version of RoSE was written during the PhD of A. Potter in 2012 to model rotation and magnetic field evolution in massive stars. Since then, we have modified it to be more stable, especially for low-mass stars and during the late phases of evolution.

The code is based on the Cambridge stellar evolution code, which we refer to as STARS. This code was originally developed by Eggleton (1971) and has been revised and improved during the past 40 yr (see in particular Pols et al. 1995; Stancliffe & Eldridge 2009). It is written in FORTRAN 77 and is approximately 7000 lines long. Details of the latest stellar physics are given by Stancliffe & Eldridge (2009). Succinctly, the code computes the stellar structure and chemical evolution simultaneously with a Newton–Raphson algorithm.

The structure and composition of the modelled star are calculated on a one-dimensional sequence of mesh points. The mesh is non-Lagrangian and the points are distributed uniformly in a spacing Q , a rather complicated function of pressure, temperature, mass, radius and density of the star. This arranges the mesh points so that higher resolution can be obtained where it is needed, such as near the burning shells in giants. This mesh-spacing function can quite easily be modified when new features are added.

The RoSE code includes additional equations for the evolution in one dimension of the effective radius r within the star, angular velocity $\Omega(r)$ and two components of the large-scale magnetic field $B_p(r)$, representing an averaged poloidal field, and included by a magnetic potential $A(r)$, and B_{ϕ} , representing an averaged toroidal field. Because the STARS code is one-dimensional we cannot model angular variations of either Ω or \mathbf{B} . This is certainly a significant approximation but one that remains necessary until full stellar evolution in two or three dimensions is possible. We also want to follow evolution over the nuclear lifetime of the star and so cannot model short term variations in either Ω or \mathbf{B} . This excludes any form of dynamo cycle from our models. We therefore require that Ω , A and B_{ϕ} remain positive throughout the evolution and so represent an average magnitude over any small-scale, short-term evolution.

2 ROTATING STARS

We know that, owing to its rotation, the Earth is not a sphere but is slightly distorted. Its equatorial radius is about 21 km longer than its polar radius. Relatively, some stars rotate much faster. In the most extreme cases the equatorial radius of a star can be up to about 1.5 times the polar radius. This deformation is caused by the centrifugal force, that also affects the internal hydrostatic balance of the star. Furthermore, helioseismology has shown that the sun does not rotate as a solid body but undergoes differential rotation. Therefore, our model assumes that the angular velocity within the interior of a star can vary. Both of these properties of stellar rotation induce internal circulation motions and instabilities that transport chemical elements and angular momentum. In this section, we describe how we modify the previous model to include the effects of rotation.

2.1 Structure equations

An important hypothesis on which we rely to derive the structure and evolution equation comes from Zahn (1992). He first assumes that stars undergo differential rotation. Because of this, he argues that the shear-driven horizontal turbulence is much stronger than the vertical turbulence.

Therefore variations in physical properties are much smaller horizontally than vertically and the angular velocity is assumed to be constant on isobaric shells. This approximation is referred to as the *shellular hypothesis*. It also applies to the state variables and composition variables. This approximation is necessary to us because it reduces a two-dimensional problem to one dimension, allowing us to easily adapt the STARS code. Let us now describe the modified equations that we use.

We define S_p to be a surface of constant pressure P , the volume contained within S_p to be V_p , r_p to be the radius of a sphere with volume V_p and m_p the mass enclosed within S_p . With these variables the mass conservation equation keeps its standard form

$$\frac{dm_p}{dr_p} = 4\pi r_p^2 \rho, \quad (1)$$

where ρ is the density on the isobaric surface.

In a rotating star the local gravity vector is

$$\mathbf{g}_{\text{eff}} = \left(-\frac{Gm_p}{r^2} + \Omega^2 r \sin^2 \theta \right) \mathbf{e}_r + \left(\Omega^2 r \sin \theta \cos \theta \right) \mathbf{e}_\theta, \quad (2)$$

where Ω is the local angular velocity, G is the gravitational constant, θ is the angle from the polar direction and \mathbf{e}_r and \mathbf{e}_θ are the radial and spherical polar unit vectors. We have neglected the effect of the aspheric mass distribution on gravity because stars are generally centrally condensed and the approximation that gravity, owing to mass, acts radially is good. To obtain one-dimensional equations, we define the average of any quantity q over S_p as

$$\langle q \rangle = \frac{1}{S_p} \int_{S_p} q d\sigma, \quad (3)$$

where $d\sigma$ is a surface element of S_p . With this notation, and according to the derivation of [Maeder \(2009\)](#), the equation of hydrostatic equilibrium becomes

$$\frac{dP}{dm_p} = -\frac{Gm_p}{4\pi r_p^4} f_p, \quad (4)$$

where P is the pressure and

$$f_p = \frac{4\pi r_p^4}{Gm_p S_p} \langle g_{\text{eff}}^{-1} \rangle^{-1}. \quad (5)$$

That is the standard hydrostatic equation is adjusted by a factor f_p which tends to unity for non-rotating stars.

In a similar way the equation for radiative equilibrium is modified to

$$\frac{d \log T}{d \log P} = \frac{3\kappa P L_p}{16\pi a c G m_p T^4} \frac{f_T}{f_p}, \quad (6)$$

where T is the temperature, κ is the opacity, a is the radiation constant, c is the speed of light, L_p is the total energy flux through S_p and

$$f_T = \left(\frac{4\pi r_p^2}{S_p} \right) \left(\langle g_{\text{eff}} \rangle \langle g_{\text{eff}}^{-1} \rangle \right)^{-1}, \quad (7)$$

again the same as in the non-rotating case except for the multiplication by f_T/f_p , which also tends to unity as the rotation vanishes.

In a non-rotating star in hydrostatic equilibrium, the transport of angular momentum and of chemical elements

would be purely diffusive. However, according to von Zeipel's theorem ([1924](#)), the thermal flux F through a point in a rotating star behaves as $F \propto g_{\text{eff}}(\theta)$. Because g_{eff} depends strongly on co-latitude θ there is a thermal imbalance that drives a meridional circulation. We introduce the meridional circulation of [Maeder & Zahn \(1998\)](#)

$$\mathbf{U} = U(r) P_2(\cos \theta) \mathbf{e}_r + V(r) \frac{dP_2(\cos \theta)}{d\theta} \mathbf{e}_\theta, \quad (8)$$

where U and V are linked by the continuity equation so that

$$V = \frac{1}{6\rho r} \frac{d}{dr} (\rho r^2 U) \quad (9)$$

and P_2 is the second Legendre polynomial $P_2(x) = \frac{1}{2}(3x^2 - 1)$. An approximate expression for U is

$$U = C_0 \frac{L}{m_{\text{eff}} g_{\text{eff}}} \frac{P}{C_p \rho T} \frac{1}{\nabla_{\text{ad}} - \nabla_r + \nabla_\mu} \left(1 - \frac{\epsilon}{\epsilon_m} - \frac{\Omega^2}{2\pi G \rho} \right) \left(\frac{4\pi^2 r^3}{3Gm} \right), \quad (10)$$

where L is the stellar luminosity, C_0 is a constant used for calibration, $m_{\text{eff}} = m \left(1 - \frac{\Omega^2}{2\pi G \rho} \right)$, $\epsilon = E_{\text{nuc}} + E_{\text{grav}}$ is the total local energy emission, $\epsilon_m = L/m$, C_p is the specific heat capacity at constant pressure, ∇_{ad} and ∇_r are the adiabatic and radiative temperature gradients and $\nabla_\mu = \frac{d \log \mu}{d \log P}$ is the mean molecular weight gradient.

We expect enhanced mass loss owing to rotation. [Friend & Abbott \(1986\)](#) suggested that near-critical rotation drives mass loss to remove angular momentum and prevents the surface from reaching critical velocity. For a star of mass M and radius R we modify the not rotating mass-loss rate $\dot{M}_{\Omega=0}$ of [Reimers \(1975\)](#) according to [Langer \(1998\)](#),

$$\dot{M} = \dot{M}_{\Omega=0} \left(\frac{1}{1 - \frac{\Omega}{\Omega_{\text{crit}}}} \right)^\xi, \quad (11)$$

where $\Omega_{\text{crit}} = \sqrt{\frac{2GM}{3R^3}}$ and $\xi = 0.45$. In subsequent sections, we drop the suffix p on r_p and m_p for ease of reading.

2.2 Angular momentum transport

Shear creates stress, and therefore dissipates energy, so a star tends towards its lowest energy state of solid body rotation. Because differential rotation is induced by, among other factors, hydrostatic structural evolution, mass loss and meridional circulation, we expect stars to be subject to a number of local hydrodynamic instabilities. The most important for us the shear instability, which occurs when there is a velocity difference between two layers of a fluid that have different properties. We assume that it dominates the vertical instabilities. The instability drives turbulence that leads to diffusion of radial and latitudinal variations in the angular velocity to bring the star back to its lowest energy state. This occurs with characteristic diffusion coefficients D_{shear} , for the shear instability acting vertically, and D_{h} for horizontal turbulence. In the shellular hypothesis, we assume that the turbulent mixing caused by these instabilities is much stronger horizontally than vertically, so that $D_{\text{h}} \gg D_{\text{shear}}$.

Including all these processes and using Zahn's ([1992](#)) formulation, we obtain the diffusion–advection equation

used to describe the evolution of angular momentum

$$\begin{aligned} \frac{\partial(r^2\Omega)}{\partial t} &= \frac{1}{5\rho r^2} \frac{\partial(\rho r^4 \Omega U)}{\partial r} + \frac{1}{\rho r^2} \frac{\partial}{\partial r} \left(\rho D_{\text{shear}} r^4 \frac{\partial \Omega}{\partial r} \right) \\ &+ \frac{1}{\rho r^2} \frac{\partial}{\partial r} \left(\rho D_{\text{con}} r^{2+n} \frac{\partial r^{2-n} \Omega}{\partial r} \right), \end{aligned} \quad (12)$$

where D_{con} is the convective diffusion coefficient and the parameter n is chosen to tend toward either solid body rotation or uniform angular momentum in the convective zones when respectively $n = 2$ or $n = 0$. To obtain the boundary conditions for the angular momentum, we integrate this equation over the star and get

$$\frac{dH_{\text{tot}}}{dt} = 4\pi r^4 D_{\text{shear}} \rho \frac{\partial \Omega}{\partial r} \Big|_0^R, \quad (13)$$

where H_{tot} is the total angular momentum. So, to ensure angular momentum conservation, we require $\frac{\partial \Omega}{\partial r} = 0$ at the surface and the centre. This condition is modified in presence of magnetic braking.

The equations for the chemical evolution are

$$\frac{\partial X_i}{\partial t} = \frac{1}{r^2} \frac{\partial}{\partial r} \left((D_{\text{shear}} + D_{\text{eff}} + D_{\Omega=0} + D_{\text{con}}) r^2 \frac{\partial X_i}{\partial r} \right), \quad (14)$$

where X_i is the mass fraction of element i . We take $D_{\text{con}} = (C_{\text{con}}(\nabla_r - \nabla_{\text{ad}})^2 m^2) / \tau_{\text{nuc}}$, where C_{con} is a large constant calculated from mixing-length theory and τ_{nuc} is the nuclear time scale. The coefficient D_{eff} describes the effective diffusion of chemical elements owing to the interaction between horizontal diffusion and meridional circulation. Again according to Zahn (1992), we take

$$D_{\text{eff}} = \frac{|rU|^2}{30D_h}. \quad (15)$$

Finally, $D_{\Omega=0}$ is the diffusion coefficient for chemical evolution without rotation. It includes simple diffusion processes, computed according to Paquette et al. (1986), convective overshooting, as included in the code by Schröder, Pols & Eggleton (1997) and semiconvection as implemented by Eggleton (1972). The coefficient D_{con} is non-zero only in convective zones and D_{shear} and D_{eff} are non-zero in radiative zones. We use the D_{shear} of Talon et al. (1997),

$$D_{\text{shear}} = \frac{2Ri_c (r \frac{d\Omega}{dr})^2}{N_T^2 / (K + D_h) + N_\mu^2 / D_h}, \quad (16)$$

where $Ri_c = (0.8836)^2 / 2$ is the critical Richardson number (Maeder 2003), K is the radiative diffusivity and the Brunt-Väisälä frequency has been split into

$$N_T^2 = -\frac{g_{\text{eff}}}{H_p} \left(\frac{\partial \ln \rho}{\partial \ln T} \right)_{P,\mu} (\nabla_{\text{ad}} - \nabla), \quad (17)$$

where ∇ is the local temperature gradient, and

$$N_\mu^2 = -\frac{g_{\text{eff}}}{H_p} \left(\frac{\partial \ln \rho}{\partial \ln \mu} \right)_{P,T} \frac{d \ln \mu}{d \ln P}, \quad (18)$$

where H_p is the pressure scale-height and μ is the chemical potential. Following Maeder (2003), we set the horizontal turbulence diffusion coefficient to

$$D_h = 0.134 r (r \Omega V (2V - \alpha U))^{1/3}, \quad (19)$$

where

$$\alpha = \frac{1}{2} \frac{d(r^2 \Omega)}{dr}. \quad (20)$$

2.3 Numerical implementation

Rotation is included in the STARS code by adding a new second-order finite difference equation. The chemical evolution equations are also modified to include the new diffusion coefficients and the structure equations include the f_T and f_p multiplicative coefficients.

The RoSE code (Potter et al. 2012a) was quite unstable, requiring a number of approximations to ensure stability throughout the evolution. The solver often produced negative solutions for angular momentum in some sections of the star, creating excessive shear that led to the instability. To solve this problem, the perturbed solution used in the Newton-Raphson solver is adapted so that, at each time step and for every iteration of the solution, the angular velocity cannot become negative. This has the effect of greatly improving the stability and reduces the number of approximations needed.

Most of the approximation consisted of addition of constant diffusion coefficients in certain zones, near the core and the surface, to ensure that sudden changes in behaviour at the boundaries could be limited. This was done with functions of the form

$$f(x, x_0, \sigma) = \frac{1}{2} \left(1 - \tanh \left(\frac{x - x_0}{\sigma} \right) \right). \quad (21)$$

Because each of these approximations requires three parameters, two for the function f and a diffusion coefficient, they introduced many degrees of freedom and required fine tuning to ensure convergence. We have eliminated the need for all but one of these.

Other approximations consisted of limiting certain quantities, such as the amount of shear. These have all been removed now. Finally, the coefficient D_{con} could be non-zero in non-convective regions. This also created instability and was not physically acceptable. To avoid this we create a smooth transition to zero for the diffusion coefficients at the boundary between the radiative zones and the convective zones. For example, if we call D'_{con} the coefficient that is calculated in the whole star, the coefficient we use is given by

$$D_{\text{con}} = D'_{\text{con}} \times f(\nabla_r - \nabla_{\text{ad}}, 0, \nabla_c), \quad (22)$$

where ∇_c is a fixed characteristic gradient. This cannot be too small because a transition that is too sharp creates discontinuities that make the code unstable nor too high as to make the results not physically acceptable. We use the same method for the coefficients D_{shear} and D_{eff} , by multiplying by $1 - f(\nabla_r - \nabla_{\text{ad}}, 0, \nabla_c)$. With these modifications, the RoSE code without any magnetic field is much more stable.

3 STELLAR MAGNETISM

Previously, most of the models for magnetism in stellar evolution took magnetic field as a function of the angular momentum in stellar interior. A particularity of RoSE and the models presented here is that the toroidal and poloidal components of the magnetic field are evolved as independent variables, thanks to two advection-diffusion equations. These equations couple rotation and the two components of the field through the magneto-rotational instability and a simple $\alpha - \Omega$ dynamo. Dynamo mechanisms are studied in

the frame of mean field magnetohydrodynamics, developed for example by Moffatt (1970), and we follow the method of Roberts (1972) for the derivation of the dynamo. In a similar way to the evolution of the angular momentum, we derive these equations by assuming that turbulence from rotational and magneto-rotational instabilities leads to the diffusion of the magnetic field and of the angular momentum, as well as generation of magnetic field by the dynamo.

3.1 Magnetic field evolution

The magnetic field in the interior of a star is coupled to the fluid movements through magnetohydrodynamics. First, we once again assume the velocity field is of the form

$$\mathbf{U} = U(r)P_2(\cos\theta)\mathbf{e}_r + V(r)\frac{dP_2(\cos\theta)}{d\theta}\mathbf{e}_\theta \quad (23)$$

and take $U(r)$ as before (equation 8). In mean field magnetohydrodynamics, we assume that the fields can be decomposed into large- and small-scale components. The evolution of the large-scale magnetic field is described by the induction equation

$$\frac{\partial \mathbf{B}}{\partial t} = \nabla \times (\mathbf{U} \times \mathbf{B}) - \nabla \times (\eta \nabla \times \mathbf{B}), \quad (24)$$

where η is the magnetic diffusivity. The magnetic field \mathbf{B} can be decomposed into a toroidal and a poloidal component,

$$\mathbf{B} = B_\phi(r, \theta)\mathbf{e}_\phi + \nabla \times (A(r, \theta)\mathbf{e}_\phi), \quad (25)$$

where B_ϕ and A give the toroidal and poloidal fields. Equations (23) and (24) become

$$\begin{aligned} \frac{\partial B_\phi}{\partial t} &= rB_r \sin\theta \frac{\partial \Omega}{\partial r} + B_\theta \sin\theta \frac{\partial \Omega}{\partial \theta} \\ &\quad - \frac{1}{r} \frac{\partial}{\partial \theta} \left(V(r) \frac{dP_2(\cos\theta)}{d\theta} B_\phi \right) - \frac{1}{r} \frac{\partial}{\partial r} (rU(r)P_2(\cos\theta)B_\phi) \\ &\quad - (\nabla \times (\eta \nabla \times \mathbf{B}))_\phi \end{aligned} \quad (26)$$

and

$$\begin{aligned} \frac{\partial A}{\partial t} &= -\frac{2V(r)}{r} \frac{dP_2(\cos\theta)}{d\theta} A \cot\theta - \frac{U(r)P_2(\cos\theta)}{r} \frac{\partial(rA)}{\partial r} \sin\theta \\ &\quad + \alpha B_\phi - \nabla \times (\eta \nabla \times A \mathbf{e}_\phi)_\phi, \end{aligned} \quad (27)$$

where an α term has been introduced in the last equation to describe the regeneration of poloidal field by a dynamo. With the shellular hypothesis, the term $B_\theta \sin\theta \frac{\partial \Omega}{\partial \theta}$ vanishes.

We must reduce these equations to one dimension to include them in the stellar evolution code. So we choose the θ dependence of the magnetic field and perform a suitable latitudinal average of the evolution equations for its two components. We choose $A(r, \theta) = \tilde{A}(r) \sin\theta$ so that, in the purely diffusive limit, the poloidal field tends towards a dipolar geometry. From the imposed form of the magnetic field, we obtain $B_r = \frac{2\tilde{A} \cos\theta}{r}$ and $B_\theta = -\frac{d(\tilde{A})}{dr} \sin\theta$. We also want the toroidal field to vanish at the poles to avoid singularities, so that we choose $B_\phi = \tilde{B}_\phi(r) \sin(2\theta)$. These choices are not unique but are the simplest we can make that respect our requirements. Finally, we take $\alpha = \tilde{\alpha}(r)$ and $\eta = \tilde{\eta}(r)$. We

then define a new average of a quantity q to be

$$\langle q \rangle_{\text{mag}} = \int_0^{\pi/2} q \sin\theta d\theta. \quad (28)$$

Averaging the evolution equations and using the chosen forms for the components of the magnetic field, we obtain the one-dimensional equations we need,

$$\frac{\partial B_\phi}{\partial t} = A \frac{\partial \Omega}{\partial r} - \frac{6}{5r} V B_\phi - \frac{1}{10r} U B_\phi + r \frac{\partial}{\partial r} \left(\frac{\eta}{r^4} \frac{\partial}{\partial r} (r^3 B_\phi) \right) \quad (29)$$

and

$$\frac{\partial A}{\partial t} = \frac{3V}{2r} A - \frac{U}{8r} \frac{\partial}{\partial r} (Ar) + \frac{8\alpha}{3\pi} B_\phi + \frac{\partial}{\partial r} \left(\frac{\eta}{r^2} \frac{\partial}{\partial r} (r^2 A) \right). \quad (30)$$

For the boundary conditions, we take the case where diffusion dominates the other terms, so that $A \propto 1/r^2$ and $B_\phi \propto 1/r^3$ as $\eta \rightarrow \infty$. This is what we expect for a dipolar field, so that we assume that $B_\phi = 0$ and $B_\theta \propto \frac{\partial(rA)}{\partial r}$ at $r = 0$ and R .

3.2 Angular momentum evolution with magnetic field

We extend the evolution equation (12) for the angular momentum using the formulation of Spruit (2002). In this model, the transport of angular momentum is driven by the Maxwell stress produced by the magnetic field. This process is assumed to be diffusive and so the equation becomes

$$\begin{aligned} \frac{\partial r^2 \Omega}{\partial t} &= \frac{1}{5\rho r^2} \frac{\partial(\rho r^4 \Omega U)}{\partial r} + \frac{3r}{8\pi\rho} \langle (\nabla \times \mathbf{B}) \times \mathbf{B} \rangle_\phi \\ &\quad + \frac{1}{\rho r^2} \frac{\partial}{\partial r} \left(\rho D_{\text{tot}} r^4 \frac{\partial \Omega}{\partial r} \right), \end{aligned} \quad (31)$$

where the term D_{tot} now includes magneto-rotational turbulence as well as rotationally-driven turbulence and convection. The purely hydrodynamic turbulence comes from shear instabilities. We absorb the effective diffusion coefficient D_{eff} in D_{shear} . The diffusion coefficient for convective transport is D_{con} and we call D_{mag} the magnetic diffusion coefficient (section 3.3). The total diffusion coefficient includes all these effects, $D_{\text{tot}} = D_{\text{shear}} + D_{\text{con}} + D_{\text{mag}}$. We have also implicitly chosen $n = 2$ so that convective turbulence leads to a viscous shear that drives convective regions towards uniform rotation. There is no good justification for this (see Potter et al. 2012a). However differential rotation in the Sun's convective zone is latitudinal rather than radial and we cannot model this properly in our one-dimensional shellular model. Neglect of convective driving of differential rotation means that we probably underestimate magnetic field generation in convective zones. After averaging the magnetic stress term in the previous equation over θ , we find

$$\begin{aligned} \frac{\partial r^2 \Omega}{\partial t} &= \frac{1}{5\rho r^2} \frac{\partial(\rho r^4 \Omega U)}{\partial r} + \frac{3}{64\rho r^3 B_\phi} \frac{\partial}{\partial r} (r^3 B_\phi^2 A) \\ &\quad + \frac{1}{\rho r^2} \frac{\partial}{\partial r} \left(\rho D_{\text{tot}} r^4 \frac{\partial \Omega}{\partial r} \right). \end{aligned} \quad (32)$$

3.3 Magnetic diffusion

In radiative zones, angular momentum is assumed to be redistributed by magnetic turbulence driven by the Tayler in-

stability (Taylor 1973). We use the turbulent diffusion coefficients of Maeder & Meynet (2000). The magnetic diffusivity η satisfies the equation

$$\left(N_T^2 + N_\mu^2\right)\eta^2 + \left(2KN_\mu^2 - \frac{r^2\omega_A^4}{\Omega}\right)\eta - 2Kr^2\omega_A^2 = 0, \quad (33)$$

where N_T is the Brunt-Väisälä frequency, N_μ is the frequency associated with the mean molecular weight gradient, K is the thermal diffusivity and ω_A is the Alfvén frequency. The magnetic diffusivity is calculated by solving this equation.

We take the calibration constant C_m of Potter et al. (2012c) to unity. Finally, we introduce the chemical Prandtl number Pr_c and the magnetic Prandtl number Pr_m so that the chemical evolution equation becomes

$$\frac{\partial X_i}{\partial t} = \frac{1}{r^2} \frac{\partial}{\partial r} \left(\text{Pr}_c D_{\text{tot}} r^2 \frac{\partial X_i}{\partial r} \right) \quad (34)$$

and $D_{\text{mag}} = \eta/\text{Pr}_m$. The two Prandtl numbers describe how efficiently the turbulent diffusivity transports magnetic flux and chemical composition compared to angular momentum.

3.4 Dynamo model

Following Maeder & Meynet (2000) we describe the α -part of the magnetic dynamo by taking $\alpha = \gamma r/\tau_a$, where γ is an efficiency parameter and τ_a is the amplification time-scale of the field. We then use $\tau_a = \frac{N}{\omega_A \Omega q}$, where $q = \frac{\partial \log \Omega}{\partial \log r}$. This gives the dynamo efficiency

$$\alpha = \gamma \frac{r \omega_A \Omega q}{N}. \quad (35)$$

Following Potter et al. (2012c) we choose a fiducial $\gamma = 10^{-16}$ but the question of what choice of γ distinguishes between a super-critical dynamo, that generates magnetic field faster than it diffusively decays, and a sub-critical dynamo, that does not, is of interest when the sustainability of poloidal field is important. We address this empirically at the start of section 4.4 and deduce that our fiducial choice is significantly super-critical. We note again that we are modelling neither the latitudinal variation of the magnetic field nor short time-scale variations. So we cannot model magnetic cycles (Roberts 1972). Nor do we want to model cycles that have periods much less than the thermal timescale of our star.

3.5 Magnetic braking

We include magnetic braking as angular momentum is carried away by a stellar wind. Magnetic field spins down the surface of the star by effectively forcing the wind to corotate to the Alfvén radius (Mestel & Spruit 1987), at which the magnetic energy density matches the kinetic energy density in the stellar wind. We integrate equation (12) to get

$$\frac{dH_{\text{tot}}}{dt} = 4\pi R^4 \rho D_{\text{tot}} \left(\frac{\partial \Omega}{\partial r} \right)_R, \quad (36)$$

where $\frac{dH_{\text{tot}}}{dt}$ is the total rate of angular momentum loss from the star. With the formulation of Weber & Davis (1967),

$$\frac{dH_{\text{tot}}}{dt} = R_A^2 \Omega \dot{M} = \sigma^2 J_{\text{surf}}, \quad (37)$$

where R_A is the Alfvén radius, $\sigma = \max(1, \frac{R_A}{R})$ and J_{surf} is the specific angular momentum at the surface of the star. According to ud-Doula & Owocki (2002) we can calculate the magnetic efficiency

$$\phi(r) = \frac{B_*^2 R^2 \left(\frac{r}{R}\right)^{-4}}{\dot{M} v_\infty \left(1 - \frac{R}{r}\right)}, \quad (38)$$

where $v_\infty = v_{\text{esc}} = \sqrt{2g_{\text{eff}} R}$ is the escape velocity at the stellar surface. The Alfvén radius is typically taken where the dynamo efficiency is equal to one. Hence, setting $\phi = 1$ and $\sigma = R_A/R$, we obtain the equation

$$\sigma^4 - \sigma^3 = \frac{B_*^2 R^2}{\dot{M} v_{\text{esc}}}. \quad (39)$$

Potter et al. only considered the asymptotic cases of either very strong or very weak magnetic field to determine the interesting solution for of the equation (39) but we solve this with a Newton method that converges within a few steps.

3.6 Numerical implementation

Magnetic effects are implemented in a very similar way to angular momentum. Two finite difference diffusion-advection equations are derived from the evolution equations (29) and (30) and the finite difference equation for angular momentum now includes the new term describing Maxwell stress.

As for angular momentum, many approximations made by Potter et al. have been eliminated. The only diffusion coefficient that needs to be adjusted is the total diffusion coefficient for the toroidal component of the magnetic field. Because of the dipolar structure of the field, the toroidal component is much stronger near the centre of the star when the core is fully radiative. This happens at the end of the main sequence. The field can then be higher than 10^6 G at the last but one mesh point near the core. To meet the boundary condition the field then goes to zero within one mesh point. This creates a discontinuity that makes the code unstable. Hence, we apply a quite important extra diffusion to the five mesh points closest to the centre to ensure stability. Varying this fixed coefficient on the main sequence has shown that it has no effect on the evolution of the magnetic field.

Once again, preventing negative angular momentum makes the code much more stable. With sufficient precision, it is now possible to simulate the entire life of most stars given an initial magnetic field and angular velocity.

4 RESULTS

We investigate the origin and evolution of large-scale magnetic fields in intermediate mass stars. Because A and B stars are observed with various magnetic fields covering a few decades in their surface intensity, it is interesting to see whether variations in the initial magnetic fields and rotation can reproduce the diversity of the observed fields.

4.1 Free parameters and initial model

We simulate the evolution of a $3 M_\odot$ star at solar metallicity $Z = 0.02$. The magnetic Prandtl number is fixed to

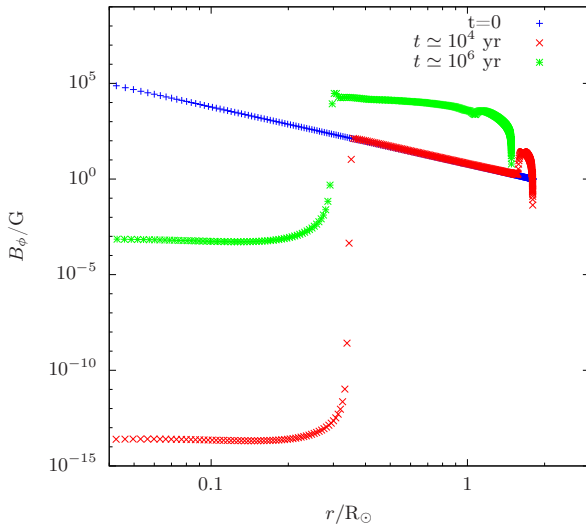


Figure 1. The toroidal field at different times during pre-mainsequence evolution. The large-scale field is completely expelled from the convective core and is roughly dipolar in the radiative zone. The drop at the surface is due to the boundary conditions. At $t = 10^6$ yr the star has reached the zero-age main sequence.

$\text{Pr}_m = 1$, the chemical Prandtl number is fixed to $\text{Pr}_c = 0.01$ to match the constraints on terminal-age main-sequence nitrogen enrichment determined by Hunter et al. (2009). To explore the properties of the α -dynamo effect we vary the initial field and the initial stellar spin rate. The parameter n has a strong influence on the result, because $n = 0$ produces uniform angular momentum in the convective zone and this results in large shears throughout these zones.

Given an initial equatorial surface speed v_{ini} , we generate an initial model that has homogeneous composition and has reached thermal equilibrium through contraction. It also has either uniform angular momentum if $n = 0$ or solid body rotation if $n = 2$, such that the surface velocity matches our needs. As long as they are reasonable enough to ensure the stability of the code, different magnetic fields can be added to our model. Because we expect the field to be approximately dipolar in the zones where it can be sustained, we choose the initial fields to behave as $B_\theta \propto r^{-3}$ for the toroidal field and $A \propto r^{-2}$. The initial strength of the poloidal field, or more precisely of A/r , is chosen to be a few orders of magnitude smaller than the strength of the toroidal field. This choice is motivated by the simulated results, which indicate that the poloidal component is often much smaller than the toroidal and this usually leads to numerical stability.

4.2 Pre-mainsequence evolution

Our initial models are $3 M_\odot$ stars towards the end of their pre-mainsequence evolution. They have a radiative envelope and convective core of approximately $0.7 M_\odot$ and of radius $0.35 R_\odot$, with variations of less than 1 per cent between the non-rotating models and models at half of the critical rotation rate. From these models our simulated evolution tracks begin before any nuclear reactions affect the stellar struc-

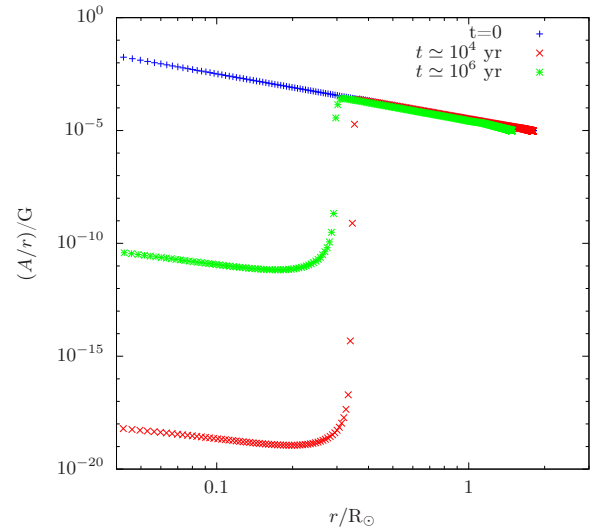


Figure 2. The poloidal field at different times during pre-mainsequence evolution. The large-scale field is also completely expelled from the core. The field behaves as $(A/r) \propto r^{-2}$ in the radiative zone, so we expect diffusion to be the dominant process there.

ture. This allows the magnetic field to rearrange itself to its most favoured form before the beginning of the main sequence. To illustrate the field evolution within this period, we simulate the evolution of a $3 M_\odot$ star, with $n = 2$. Initially, the star is on the pre-mainsequence, and is in corotation, that is to say with uniform angular velocity. The initial surface rotation speed is 100 km s^{-1} . The components of the magnetic field are such that the field is initially dipolar. The initial surface strength of the toroidal component is 1 G and we choose $A/r = 10^{-5} \text{ G}$ at the surface. The α -dynamo efficiency is fixed to $\gamma = 10^{-16}$. Figs 1 and 2 show the two components at the beginning of the evolution, after approximately 10,000 yr and at the beginning of the main sequence, approximately 10^6 yr later.

Within the first ten thousand years both components of the large-scale field are completely dissipated in the convective core. This is due to the very large D_{con} in the convective zones. In the radiative zones, the poloidal component still behaves as $B_\theta \propto r^{-2}$. Because the angular velocity varies throughout the star creating shear, the toroidal component does not behave exactly as the poloidal component. It is roughly dipolar, except near the surface where magnetic braking results in shears that increase the field, before it falls to zero within a very narrow region to meet the boundary condition. The extra magnetic field is then diffused throughout the radiative envelope. The size of this bump increases with the initial poloidal field because it is sheared into toroidal. At the beginning of the main sequence, because the star has contracted and because of the Ω -dynamo effect, the toroidal field is much stronger than initially. However, the poloidal component is nearly unchanged in its strength, smaller than the toroidal component by about nine orders of magnitude. This is because the Ω -dynamo effect, which converts the shear energy into toroidal field, operates much more efficiently than the α -dynamo effect, which regenerates the poloidal field.

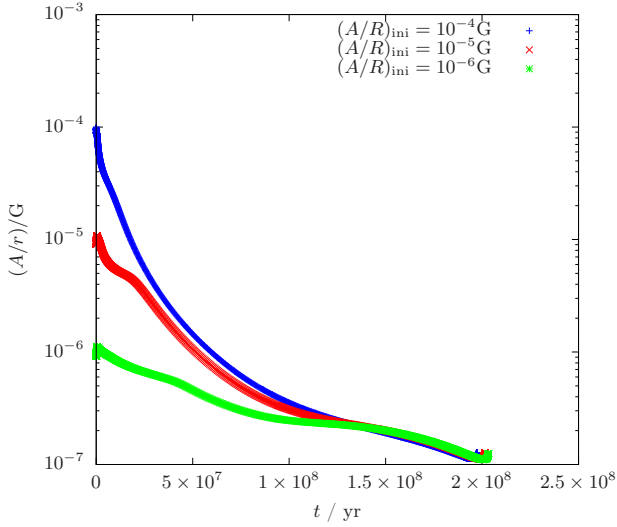


Figure 3. Surface poloidal field as a function of time during the main sequence. The initial toroidal field is dipolar and its surface strength is fixed at 1.0G. At the end of the main sequence, the field seems not to depend much on the initial field.

4.3 Main-sequence evolution

A $3 M_{\odot}$ star takes between 200 and 300 Myr to cross the main sequence and exhaust the hydrogen fuel in its core. Low- and intermediate-mass stars spend most of their lives in this phase. It is during this period that we expect to see the greatest attenuation of the field and it is crucial to see whether the initial field is completely dissipated or not.

We illustrate the main-sequence evolution of the field with similar models, but with various initial fields. All the models start in corotation. In each case, we use a dipolar initial field and vary its initial surface strength. Because of the boundary condition, the surface toroidal field always vanishes. As mentioned above, this boundary condition is met within a very narrow region near the surface and this is apparent in Fig. 1. Therefore, to describe the temporal evolution of the toroidal component, we examine a mesh point situated at $0.99R$. This is within the very narrow region of decline but close enough to the surface to allow us to observe interesting properties.

Figs 3 to 6 display the evolution of the two components of the magnetic field at or near the surface during the main sequence. Interesting common features appear when we vary the initial strength of a component, the other being initially fixed. One quite surprising point is that, at the end of the main sequence, each surface component is very close to what appears to be a common strength that does not depend on the initial strengths of the fields.

When the initial poloidal field is strong enough, the toroidal field reaches a peak at the beginning of the main sequence. It then weakens, mainly because the radius of the star increases toward the end of the main sequence. For Figs 3 and 4 we vary the initial strength of the poloidal field, the initial toroidal field being fixed and we do the converse for Figs 5 and 6. For both components, the initial poloidal field seems to have a much larger influence on the early main-sequence evolution than the initial toroidal field. Once again,

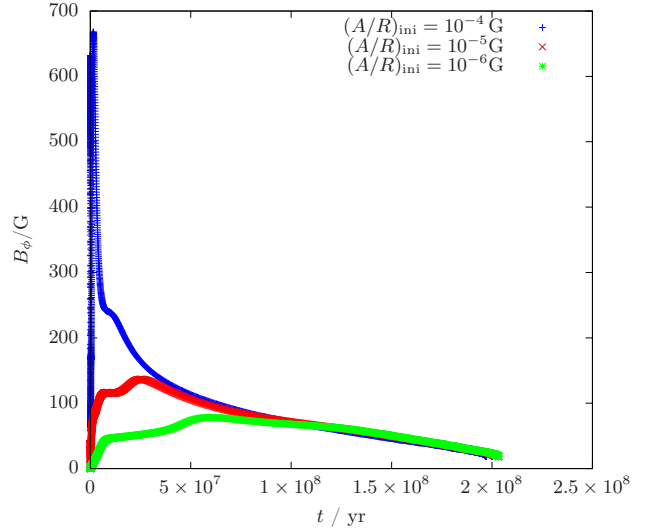


Figure 4. Evolution of the toroidal field near the surface as a function of time during the main sequence. Again the initial toroidal field is dipolar and its surface strength is fixed to 1.0G. Once again, a common field strength is met at the end of the main sequence.

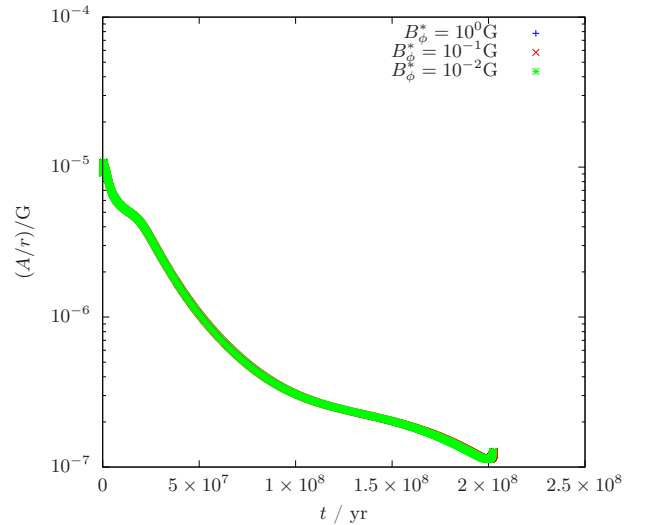


Figure 5. Surface poloidal field as a function of time during the main sequence. The initial poloidal field is dipolar and its surface strength is reduced to 10^{-5} G.

this is linked to the fact that the Ω -dynamo is more efficient than the α -dynamo at generating toroidal field.

The fact that both surface fields reach strengths that do not depend on the initial field is quite striking and this raises the same question for the fields in the interior. Figs 7 and 8 show the toroidal and poloidal components of the field at the end of the main sequence, for the same model as before, with varying strength for initial poloidal field. We choose a fixed initial toroidal field because it has much less impact on the evolution than the initial poloidal field. Once again, both components of the field are surprisingly close to each other, despite the initial poloidal field varying over two decades. Fig. 9 shows the distribution of angular velocity in the in-

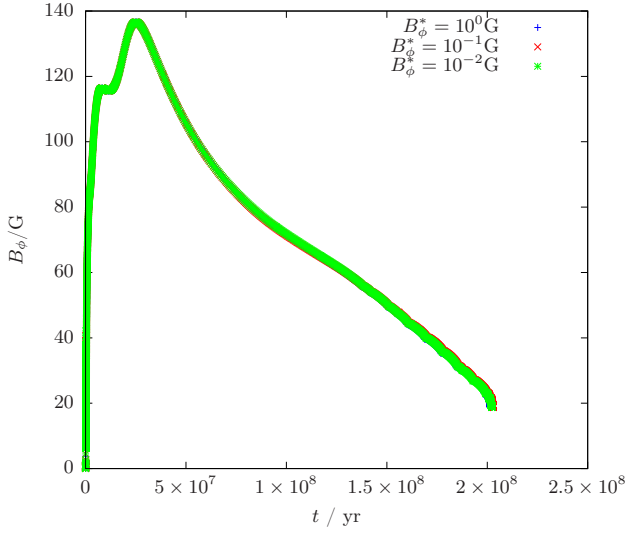


Figure 6. Evolution of the toroidal field near the surface as a function of time during the main sequence. The initial poloidal field is dipolar and its surface strength is reduced to 10^{-5} G. The initial strength of the toroidal field seems to have much less influence on the result than the initial strength of the poloidal field.

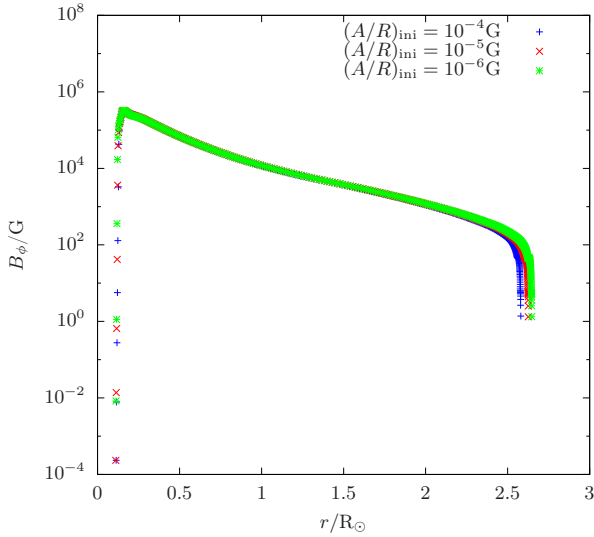


Figure 7. Toroidal field in the interior of the star as a function of the radius at the end of the main sequence.

terior of the star at the end of the main sequence for the various initial fields. The larger the initial poloidal component, the lower is the angular speed at the end of the main sequence. This is due to the fact that the Ω -dynamo effect is modelled with a term equal to $A \frac{\partial \Omega}{\partial r}$ in the toroidal field evolution equation. Hence, the higher A , the more efficiently shear energy is transferred to the magnetic field.

The fact that the magnetic field does not depend on the initial field and that the angular velocities in the interior vary significantly suggests that, given an initial velocity and with a fixed α -dynamo efficiency, there exists an equilibrium for the field in the radiative zone. This observation favours the dynamo hypothesis over the fossil field for stars in the

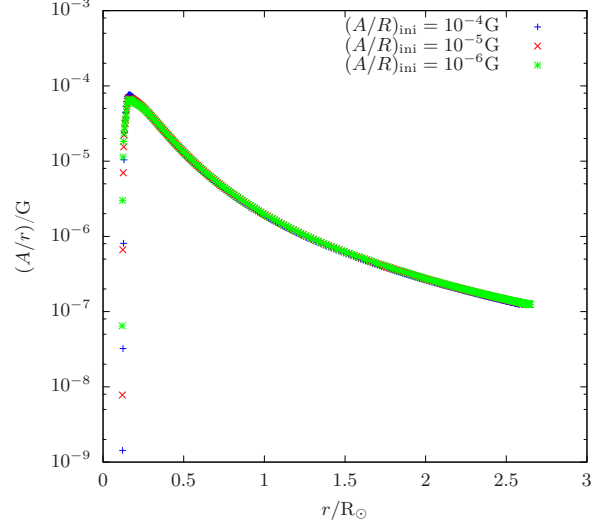


Figure 8. Poloidal field in the interior of the star as a function of the radius at the end of the main sequence.

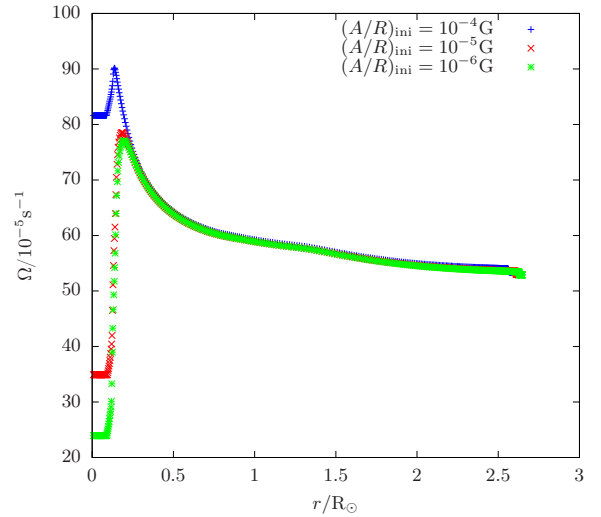


Figure 9. Angular velocity in the interior of the star as a function of the radius at the end of the main sequence for different initial surface poloidal fields. The drop at the surface is due to magnetic braking.

second half of their main sequence. Moreover, for stars that are still early on the main sequence, the initial conditions play an important role. This conclusion seems to be possibly at odds with the fact that we see both magnetic and non-magnetic A and B stars, with surface fields ranging over a few decades, but so far we have only changed the initial conditions for the components of the field.

To investigate the effects of initial rotation, we simulate the evolution of a $3 M_{\odot}$ star, with an initial dipolar field of surface strength 1 G for the toroidal component and 10^{-5} G for the poloidal component. Again, every model starts in uniform rotation. The α -dynamo efficiency is fixed to $\gamma = 10^{-16}$, we promote solid body rotation with $n = 2$ and the initial surface speed is taken to be $v \in \{1, 10, 20, 50, 100, 150\} \text{ km s}^{-1}$. A non-rotating star with the same characteristics has a

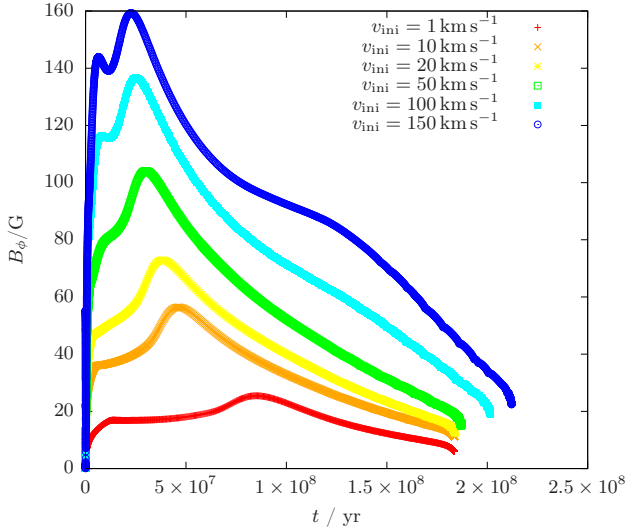


Figure 10. Toroidal field strength near the surface as a function of time during the main sequence for different initial surface speeds.

radius $R = 1.789 R_{\odot}$ so that, initially, the various models have $\Omega/\Omega_{\text{crit}} \in \{0.002, 0.02, 0.04, 0.11, 0.21, 0.33\}$, where $\Omega_{\text{crit}} = \sqrt{\frac{2GM}{3R^3}}$ (equation 11) and v and Ω are in the same ascending order. The corresponding critical velocity is $v_{\text{crit}} = R\Omega_{\text{crit}} \simeq 460 \text{ km s}^{-1}$.

Except for the lowest velocities, the behaviour of the toroidal field (Fig. 10) is roughly the same as before. It reaches a peak at the beginning of the main sequence and then weakens as time passes. As expected, the faster the star rotates, the stronger the field becomes. The intensity of the field covers approximately two decades. In addition, as seen in Fig. 4, variations of the initial strength of the poloidal field can produce variations in the intensity of the surface toroidal field over a few decades. Hence, the initial velocity of the star and its initial poloidal field appear to be the main factors that determine the intensity of the toroidal field and the combination of the two effects can produce fields with intensities of a few to over 100 G early on.

4.4 Post-mainsequence evolution

The efficiency of the α -dynamo does indeed have an influence on the intensity of the magnetic field over the main sequence. We simulate the evolution of the same star as before, with an initial dipolar field of surface strength 1 G for the toroidal component and 10^{-5} G for the poloidal component and an initial rotation speed of 100 km s^{-1} , with the efficiency parameter $\gamma \in \{10^{-14}, 10^{-15}, 10^{-16}, 10^{-18}, 10^{-19}\}$. Figs 11 to 13 show the poloidal and toroidal fields as well as the angular velocity at the end of the main sequence. As expected, the poloidal field is stronger for higher α , because more poloidal field is generated for given toroidal. By the Ω -dynamo, a higher poloidal field also results in a stronger toroidal field. Varying α produces greater changes in the strength of the poloidal field, with variations over more than two decades for the various α s, than in the strength of the toroidal field, which varies over less than a decade here. When $\gamma = 10^{-19}$

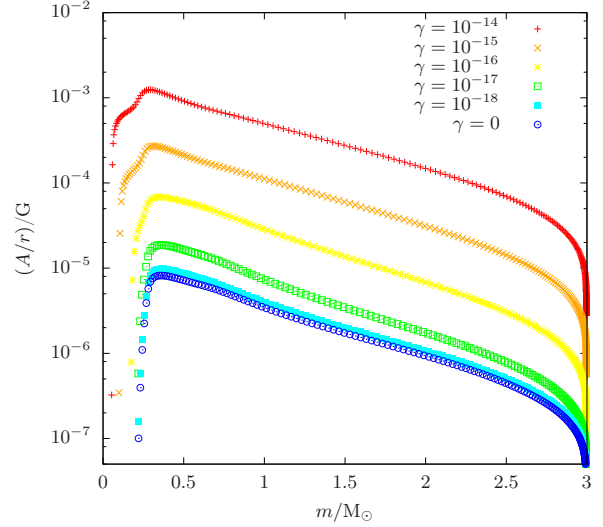


Figure 11. Poloidal field in the interior of the star as a function of radius at the end of the main sequence for various dynamo efficiencies γ .

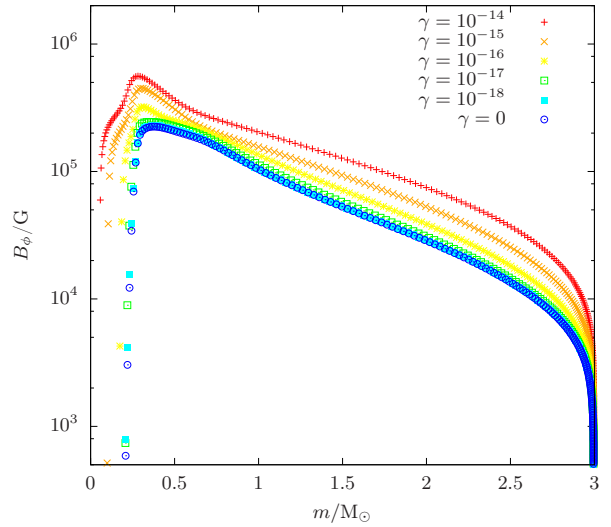


Figure 12. Toroidal field in the interior of the star as a function of the radius at the end of the main sequence for various dynamo efficiencies γ .

the magnetic field evolution is indistinguishable from when $\gamma = 0$. So we take this as an indication that $\gamma \approx 10^{-18}$ is critical and that our fiducial $\gamma = 10^{-16}$ is significantly supercritical. From equation (32), we expect the stronger poloidal field to enforce more corotation, that is uniform angular velocity. This is seen in Fig. 13, where the models with higher efficiency are much closer to uniform angular velocity than those with lower efficiency.

Finally, the magnetic field for $\gamma = 10^{-18}$ is nearly the same as the field with no α -dynamo. This suggests that there exists a minimum field strength, toward which the field tends when the α -dynamo is very inefficient compared to the other effects such as Ω -dynamo or diffusion.

After the end of the main sequence and before end-

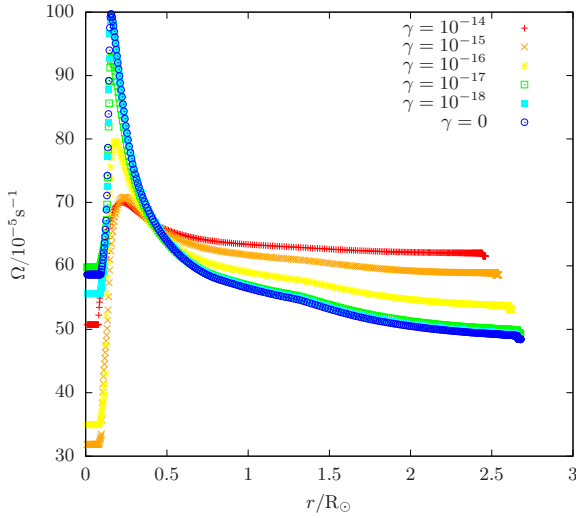


Figure 13. Angular velocity in the interior of the star as a function of the radius at the end of the main sequence for various dynamo efficiencies γ .

ing their lives as white dwarfs, low- and intermediate-mass stars undergo many very important structural changes. In the case of a $3 M_{\odot}$ star, the evolution from the end of the main sequence to the asymptotic giant branch takes roughly 70 Myr, approximately a third of the time it spends as a main-sequence star. However, if a magnetic field can be sustained throughout the main sequence, we might also expect such a field to be preserved during the late stages of evolution, or there to be at least some memory of it.

Among the structural changes that are known in stars, some regions see their convective or radiative behaviour change during the evolution. This is of particular importance because, as has been discussed for the pre-mainsequence evolution, convective transport is the main contributor to the transport of heat, composition, momentum and magnetic field. Following the ideas of [Tout, Wickramasinghe & Ferrario \(2004\)](#), we therefore expect the the magnitude of the averaged large-scale field to be attenuated in the convective zones compared to the radiative regions. They suggested that the dissipation of the field in the convective zone is due to rapid magnetic reconnection, the conversion of magnetic energy to kinetic or thermal energy through changes of the field topology. We imagine that small-scale rapidly varying magnetic field is continually generated in convective zones and that the dissipation of this leads to the enhanced magnetic activity associated with deep convective envelopes and fully convective stars ([Gregory et al. 2012](#)). This effect prevents the sustenance of any large-scale field in a convective zone which therefore appears to act as an insulator. Though our model does not include any magnetic reconnection process, the large diffusion coefficient in the convective zone produces a simple and yet satisfying model for this dissipation. Again according to [Tout et al. \(2004\)](#), this indicates that a large-scale field can be sustained as long as the star is partially radiative. In the case of a intermediate mass stars, this is the case during all of the post-mainsequence stages of evolution.

We illustrate this for a $3 M_{\odot}$ star, initially in uniform

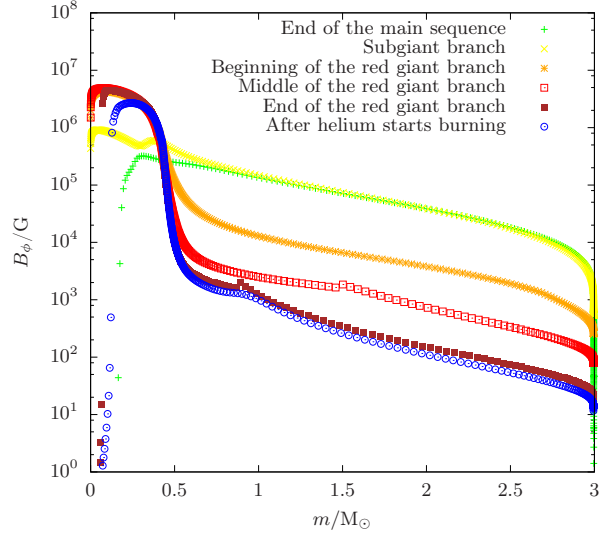


Figure 14. Toroidal field inside the star as a function of the mass at various times during the sub-giant branch and the red giant branch evolution.

rotation with an equatorial speed of 100 km s^{-1} . The initial field is dipolar, with a surface intensity of 1 G for the toroidal field and 10^{-5} G for the poloidal field. The α -dynamo efficiency is fixed with $\gamma = 10^{-16}$ and convective zones tend towards solid body rotation.

After hydrogen fuel has been completely exhausted in the centre, the star continues to burn in a thin shell around its inert helium core. During this phase, the subgiant branch, the core contracts because it is unable to produce the energy needed to prevent gravitational collapse. The core heats as it collapses, increasing the fusion rate in the hydrogen burning shell. This leads to expansion of the stellar envelope. The star cools slowly and experiences a modest increase in luminosity. During this phase, the interior becomes fully radiative, so that magnetic field can penetrate the core. The yellow points in Fig. 14 show the toroidal field during the subgiant branch phase.

As the star continues to expand, it reaches the red giant branch. Its radius can become more than a hundred times what it was in the main sequence. It also develops a convective envelope. The boundary between the convective zone and the radiative zone sees its depth increase considerably during this phase. Because of convection, the field is slowly attenuated in the outer envelope of the star and tends to concentrate near the core. This is illustrated in Fig. 14 in which the field is plotted when the star starts to ascend the red giant branch, approximately 0.3 Myr later and at the end of the red giant phase, just before helium ignites. At the end of the red giant phase, the field in the outer parts can be more than 10^6 times weaker than what it was at the end of the main sequence.

The end of the red giant phase occurs when the temperature of the core is high enough to ignite fusion of helium. At this point, the core of the star becomes convective. As on the main sequence, the field is once again expelled from the core. Because a convective envelope is still present, most of the field is then concentrated in a region just outside the helium burning core, in which the toroidal field can be lower

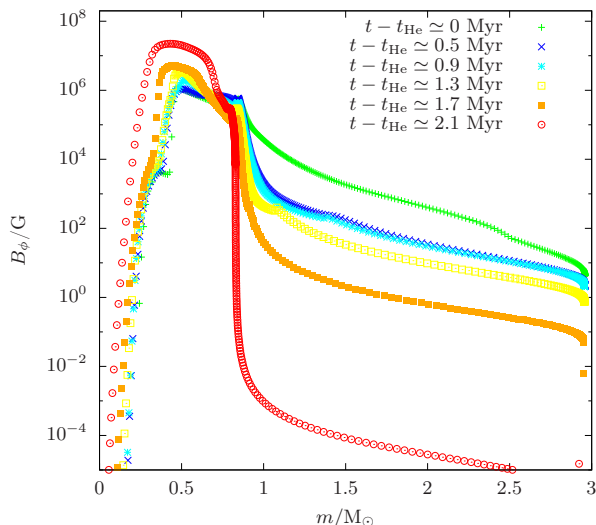


Figure 15. Toroidal field inside the star as a function of the mass coordinate at various times after helium exhaustion in the core, at time t_{He} , during the asymptotic giant phase.

than 1 G, but inside the convective envelope, where the field can be 10^5 times weaker than in the radiative region. This corresponds to the blue points in Fig. 14.

After the completion of helium burning in the core, the core starts to contract again, until it becomes degenerate. The fusion of helium and hydrogen continues in thin shells around the core, as for hydrogen in the subgiant branch. This phase is the asymptotic giant branch (AGB). Shortly after the core has exhausted its helium fuel, it becomes radiative again, so that the inner layers of the star, including the degenerate core, are contained in a radiative core and the outer regions again become a deep convective envelope.

At the end of the AGB phase, the field is almost completely contained within the degenerate core of approximately $0.75 M_{\odot}$, the only remaining radiative zone. The core is extremely compact and its radius is less than 0.001 per cent of the star but it contains 20 per cent of the total mass of the star. Hence, we expect the field to be extremely high in this zone. In our case, the toroidal component sees its strength reach between 10^6 and 10^8 G. In the convective zone, the large-scale magnetic fields are extremely weak: they can be more than 10^{10} times weaker than in the core. This is illustrated in Fig. 15, where the toroidal field is plotted as function of the mass coordinate at various times during the AGB phase. As time passes, we see that the field in the envelope is strongly attenuated, becoming negligible towards the end of this period. Once again the field concentrates in the core but without filling it entirely because the almost superconductivity of very degenerate material makes it hard for the magnetic field to diffuse to the centre. On the other hand, the outer half of the core by mass is permeated with an extremely strong magnetic field, with strength as high as 10^8 G.

4.5 Magnetic field in white dwarfs

We recall that white dwarfs form at the end of the lives of low- and intermediate-mass stars. They are remnants of

the degenerate cores that form in the late stages of stellar evolution. The previous example with the $3 M_{\odot}$ star seems to support the hypothesis of [Tout et al. \(2004\)](#) concerning the formation of very high magnetic field in white dwarfs. Through the different stages of its evolution, the studied star never became fully convective. This allowed the field to be preserved as it is transported into the radiative zones. In particular, during the final stages of their evolution, intermediate mass stars develop a convective envelope. This has the effect of concentrating the magnetic field in the degenerate core. Because this degenerate region is extremely small compared to the original size of the star, magnetic flux conservation means that the field inside the core becomes extremely high. This could be a possible explanation for the very high magnetic fields observed in some white dwarfs.

Yet, this is inconsistent with the fact that no high-field magnetic white dwarfs have been observed in wide binaries, as reported by [Tout et al. \(2008\)](#). If such high magnetic field results from the isolated evolution of a single star, we would expect to find the same fraction of high field white dwarfs among binaries as among single stars. Because this is not the case, [Tout et al.](#) suggested that the high fields are likely to be found only in cataclysmic variables ([Warner 1995](#)) or single white dwarfs derived from merged binary stars. This is still an open problem that must be further examined in the future.

White dwarfs have been observed with fields covering many decades, from non-magnetic to more than 10^9 G. Let us now explore a few possibilities to explain the diversity of the observed fields. Before they start their main-sequence evolution, stars less massive than two solar masses undergo a phase where they become fully convective. During that period, we expect the decay of large-scale magnetic field to be greatly enhanced and we are therefore less likely to observe magnetic field in these stars. Because low-mass stars also end up their lives as white dwarfs, this could explain why non-magnetic white dwarfs are common.

Our code does not allow us to easily produce white dwarfs and the evolution generally ends in the late stages of the asymptotic giant branch. Therefore, to try to evaluate the influence of the magnetic field during the main sequence on the magnetic field obtained in the degenerate core at the end of the evolution, we have evolved some of the different models shown in Fig. 10, as well as other models with the same characteristics but different initial spins, to the end of their lives. Their initial equatorial speeds are $v \in \{1, 50, 150, 250, 300, 350\} \text{ km s}^{-1}$, corresponding to $\Omega/\Omega_{\text{crit}} \in \{0.002, 0.11, 0.33, 0.54, 0.65, 0.75\}$. The toroidal fields obtained in the degenerate core are presented in Fig. 16.

The field does not completely fill the degenerate core but decreases towards the centre. As expected, the strength of the field increases as the initial rotation speed increases, but only for speeds below approximately half of the critical rotation speed. For higher angular velocities, the strength of the field decreases with angular velocity. Furthermore, the higher the field, the larger the fraction of the core that is permeated by the field. We obtained surface toroidal fields that cover nearly a decade in strength, between 10^6 and 10^8 G. White dwarfs with such fields are considered to be highly magnetic, even though the initial fields were not very intense.

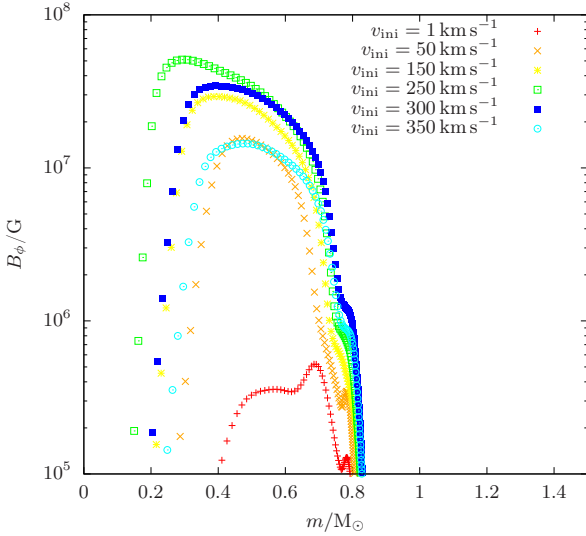


Figure 16. Toroidal field in the degenerate core before the first thermal pulse as a function of the mass coordinate for different initial rotation. The field in most of the envelope has not been represented because it is completely negligible. For initial rotation velocities below approximately half of the critical rotation speed, the strength of the field increases with the velocity, and for velocities above, the strength of the field decreases.

5 CONCLUSION

Magnetism and rotation in stars are phenomena that interact strongly. We have presented a model for the evolution of angular momentum and magnetic field during the life of a star that included an α - Ω dynamo. The main feature of this model is to allow the magnetic field to evolve as two independent components, along with the evolution of the angular momentum thanks to three advection-diffusion equations.

This model, when included in the Cambridge stellar evolution code, has allowed us derive many results concerning magnetic fields throughout the life of a $3M_{\odot}$ star. Using various initial conditions for the magnetic field and the angular velocity, we have been able to reproduce the diversity of fields observed in intermediate-mass stars during their main sequence. We have also shown that our model seems to favour a dynamo origin rather than a fossil origin for the magnetic field towards the end of the main sequence and therefore also for post-main sequence stages of evolution.

During the late phases of stellar evolution, the rearrangement of the magnetic field owing to the expansion and contraction of the radiative and convective zones has confirmed the idea of [Tout et al. \(2004\)](#) that, though convective zones in stars appear to act as insulators to large-scale magnetic fields, they can be sustained in non-convective regions throughout the life of a star, as long as it does not become fully convective. Because this is the case for intermediate mass stars and because they develop a deep convective envelope in the very last stage of their evolution on the asymptotic giant branch, magnetic field concentrates in their degenerate cores. The degenerate core is extremely dense and small compared to a star on its main sequence. So magnetic flux conservation leads us to expect a very high field in the core. Our numerical simulations have allowed us to repro-

duce this, giving a possible explanation for the very high fields observed in magnetic white dwarfs.

Yet this model is not totally consistent with some observational evidence. One open problem is that no highly magnetic white dwarfs have been observed so far in wide binary star systems, even though the previous arguments should hold for stars with a companion. Further work is required to investigate the effects of binary star interaction on magnetic field and angular momentum evolution in stars.

6 ACKNOWLEDGEMENTS

LGQ is grateful to the Institute of Astronomy for hospitality during his stay. CAT thanks Churchill college for his fellowship. We thank the reviewer for helpful comments.

REFERENCES

- Eggleton P. P., 1971, *MNRAS*, **151**, 351
 Eggleton P. P., 1972, *MNRAS*, 156, 361
 Friend D. B., Abbott D. C., 1986, *ApJ*, 311, 701
 Gregory S. G., Donati J.-F., Morin J., Hussain G. A. J., Mayne N. J., Hillenbrand L. A., Jardine M., 2012, *ApJ*, 755, 97
 Hunter I., et al., 2009, *A&A*, 496, 841
 Langer N., 1998, *A&A*, **329**, 551
 Maeder A., 2003, *A&A*, 399, 263
 Maeder A., 2009, *Physics, Formation and Evolution of Rotating Stars*. Springer Berlin Heidelberg
 Maeder A., Meynet G., 2000, *A&A*, 361, 159
 Maeder A., Zahn J.-P., 1998, *A&A*, **334**, 1000
 Mestel L., Spruit H. C., 1987, *MNRAS*, **226**, 57
 Moffatt H. K., 1970, *J. Fluid Mech.*, 41, 435
 Paquette C., Pelletier C., Fontaine G., Michaud G., 1986, *ApJS*, 61, 177
 Pols O. R., Tout C. A., Eggleton P. P., Han Z., 1995, *MNRAS*, **274**, 964
 Potter A. T., 2012, PhD thesis, University of Cambridge
 Potter A. T., Tout C. A., Eldridge J. J., 2012a, *MNRAS*, 419, 748
 Potter A. T., Tout C. A., Brott I., 2012b, *MNRAS*, 423, 1221
 Potter A. T., Chitre S. M., Tout C. A., 2012c, *MNRAS*, 424, 2358
 Reimers D., 1975, *Mem. Soc. R. Sci. Liege*, **8**, 369
 Roberts P. H., 1972, *Phil. Trans. R. Soc. A*, 272, 663
 Schröder K.-P., Pols O. R., Eggleton P. P., 1997, *MNRAS*, **285**, 696
 Spruit H. C., 2002, *A&A*, 381, 923
 Stancliffe R. J., Eldridge J. J., 2009, *MNRAS*, **396**, 1699
 Talon S., Zahn J.-P., Maeder A., Meynet G., 1997, *A&A*, **322**, 209
 Tayler R. J., 1973, *MNRAS*, **161**, 365
 Tout C. A., Wickramasinghe D. T., Ferrario L., 2004, *MNRAS*, 355, L13
 Tout C. A., Wickramasinghe D. T., Liebert J., Ferrario L., Pringle J. E., 2008, *MNRAS*, **387**, 897
 ud-Doula A., Owocki S. P., 2002, *ApJ*, 576, 413
 Von Zeipel H., 1924, *MNRAS*, **84**, 665
 Warner B., 1995, *Cataclysmic variable stars.* Cambridge Univ. Press, Cambridge
 Weber E. J., Davis Jr. L., 1967, *ApJ*, **148**, 217
 Zahn J.-P., 1992, *A&A*, **265**, 115

This paper has been typeset from a $\text{\TeX}/\text{\LaTeX}$ file prepared by the author.